

## Characterisation and activation of graphite mine tailings for use in cementitious binders

Surya Maruthupandian <sup>\*</sup> , Napoleana Anna Chaliasou, Sufyan Akram , Andreas Chrysanthou, Antonios Kanellopoulos 

Centre for Engineering Research, School of Physics, Engineering and Computer Science, University of Hertfordshire, Hatfield, UK

### ARTICLE INFO

#### Keywords:

Upcycling  
Mineral waste  
Graphite tailings  
Activation  
Supplementary cementitious materials

### ABSTRACT

The widespread use and production of Portland cement, amounting to 4.10 billion tonnes annually, poses challenges in acquiring quality raw materials. Also, the demands associated with the global development had led to intensified mining and production of significant quantity of mineral wastes including mine tailing. The quantity of disposed mine tailing is about 217 km<sup>3</sup> at present with a predicted annual addition of 12.30 km<sup>3</sup> to this volume. This poses major environmental, economic, social, and legal concerns. The Construction and Building materials research under Horizon 2020 program of Europe 2020 strategy promotes the materials for energy efficiency including materials with low embodied energy and materials capable of reusing a high waste content. Use of mine tailings, with a chemical and oxide composition similar to supplementary cementitious materials, in cementitious binders emerges as a potential solution to the above-mentioned problems. However, documented challenges, such as crystallinity, variations physical, chemical, and mineralogical characteristics, acid mine drainage, and heavy metal leaching, hinder its immediate use as a cement precursor. This study focuses on developing a suitable treatment for a siliceous mine tailing from graphite mining for its use as a binder precursor. In this study, mineralogical and activation data are presented with respect to graphite tailings. Mechanical and thermal activation protocols were developed, and the processed tailings were assessed in terms of their physico-chemical properties. The mine tailing exhibited high SiO<sub>2</sub> composition 58.5 % and was predominantly crystalline. The XRD analysis indicated the possibility of activation by milling and calcination. The characteristics and reactivity of activated samples indicated that the samples calcined at 850 °C exhibited higher heat of hydration in R3 tests and samples milled for 90 min exhibited higher solubility in alkaline environment.

### 1. Introduction

Concrete is the most widely used construction material and the second most used material in the world, with only water exceeding its consumption. Concrete's existence and quality are of primary importance for the development of robust civil infrastructure assets, which in turn support the growth and development of our society. However, concrete and most specifically its binding compound, cement, have a significant environmental footprint both in terms of CO<sub>2</sub> emissions and in relation to the depletion of natural resources. Global demand for cement is projected to yield a rise on its production to a staggering 5 Gt over the next 30 years [1]. That amounts to about 20 % increase from the current production levels. In recent years, the importance for transformation in the sector has been strongly proposed. For example, the International Energy Agency, in its recently published roadmap for a

sustainable transition in the cement and concrete industries, has strongly highlighted two important actions: (i) the need to switch to alternative raw materials by 2025 and (ii) to switch to alternative cementitious binders by 2035 [2]. This strategy is also promoted by the European Cement Association in its latest report on decarbonisation of cement [3]. The Institution of Civil Engineers' low carbon concrete routemap further highlights the importance of new sustainable and innovative developments for the manufacture of binders with low environmental footprint [4].

At the same time, there are billions of tones of mine tailings produced as part of the mineral separation processes in the mining sector. These waste products are typically disposed and stockpiled in landfills and pose a significant environmental liability [5–7]. The projections suggest that, as with cement, there will be significant increase of mining activities for the next 30 years [8]. Subsequently, the existing problem of

<sup>\*</sup> Corresponding author.

E-mail address: [s.maruthupandian@herts.ac.uk](mailto:s.maruthupandian@herts.ac.uk) (S. Maruthupandian).

<https://doi.org/10.1016/j.conbuildmat.2025.140923>

Received 31 October 2024; Received in revised form 13 January 2025; Accepted 16 March 2025

Available online 28 March 2025

0950-0618/© 2025 The Author(s). Published by Elsevier Ltd. This is an open access article under the CC BY license (<http://creativecommons.org/licenses/by/4.0/>).

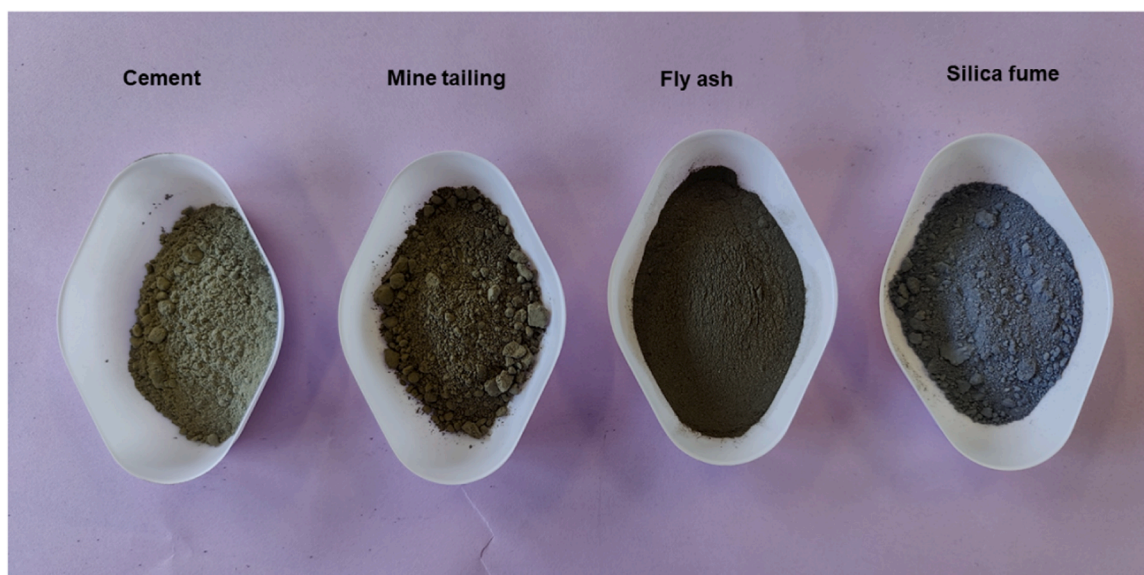


Fig. 1. Colorimetric comparison of cement, mine tailing, fly ash and silica fume.

managing tailings will be inflated to a critical point. The mineralogical similarity of tailings to raw materials used for the manufacture of cement make them an interesting candidate for their potential use as cementitious binders [9–13]. The upcycling of tailings for the production of cementitious binders can provide a solution to the significant issues of resource depletion and tailings management. However, the highly crystalline nature of tailings inhibits their uptake as binders in cement-based systems. Thermomechanical and chemical treatments are necessary to rearrange the highly ordered crystal structure of tailings to an amorphous arrangement of atoms [14]. This transformation will allow tailings to participate in the chemical reactions within a cementitious matrix.

Graphite is an allotrope of carbon with various industrial applications including batteries, lubricants, electrodes and graphene compounds. The worldwide production of graphite was about 1.10 million metric tons in the year 2020 [15]. Production of one tonne of graphite produces about 10–15 tonnes of graphite tailing [16]. However, global efforts under the aegis of climate action [17] and EU’s “Clean planet for all” [18], recommends clean energy technologies such as photovoltaic conversion, harvesting wind and thermal energy, storage of these energies, electric mobility, and digital technologies (ICT, robotics, 3D printing). Production of these technological equipment requires very high amounts of critical and non-critical minerals posing an increased demand on mining activities including graphite [18]. The production of graphite is expected to increase from 1300 kt in the year 2022 to 3550 kt in the year 2050, which may lead to increased production of more graphite mining wastes [19]. This poses a need for an urgent and more sustainable method for disposal of the graphite mining waste.

Past studies have explored different ways to use graphite tailings in construction which includes use as cement replacement and fine aggregate [9,20,21]. The graphite mine tailings are predominantly siliceous and therefore their use as source of silica has also been explored [22]. Feasibility of producing conductive concrete using carbon fibres and graphite tailing as an addition (filler) was studied [9] and it was reported that the compressive strength decreased by 5.26 % at 5 % addition and by 34.00 % at 15 % addition of untreated tailings. The study also found that the use of graphite tailing improved conductivity of concrete and recommended addition of carbon fibres to compensate for the loss in strength. The mortar made with 20, 30 and 40 % graphite tailings as sand replacement had a better resistance to freeze thaw cycle due to increased pore size which catered to the expansion of water during freezing [16]. A curing temperature of 60°C is recommended

when 40 % of fine aggregates is replaced by graphite mine tailing. It was observed that at a curing temperature of 60°C samples with tailings showed the formation of hydration products and had better early age mechanical properties than the specimens cured in standard conditions [21]. Various studies have been reported on the use of other siliceous tailings as supplementary cementitious materials [23–27] and as precursors for alkali activated cements [28–30]. The compressive strength decreased by 36.00 % with increase in percentage of tailings to 30 % [24]. However, the use of water reducing admixture improved the packing density and mechanical properties when siliceous copper coarse tailing was used [23]. The durability of concrete improved with use of coal siliceous mine tailing as a cement replacement when the percentage of replacement was 20 % [31,32]. Yao et al. [33] reported an improvement in mechanical properties with the inclusion of milled siliceous tailings. The strength ratio (strength of concrete with mine tailing to control concrete) improved from 62.70 % to 80 % after 80 min of milling, at 30 % cement replacement.

From the literature it is evident that only a very limited number of studies have dealt with the use of graphite mine tailings in cementitious binders. In addition, various researchers have followed different approaches that include the use of tailings as fillers, the use of tailings as aggregate replacement and the use of tailings as cementitious compounds. In the absence of sufficient data and the variability of the adopted methods, the reported results are either limited or not conclusive [14]. Therefore, the present study focuses developing a suitable treatment for a siliceous mine tailing from graphite mining for its use as a binder precursor. In this study, mineralogical and activation data are presented with respect to graphite tailings. Mechanical and thermal activation protocols were developed, and the processed tailings were assessed in terms of their physico-chemical properties.

## 2. Materials

### 2.1. Mine tailings

The mine tailings (MT) used in this study, were a waste product in graphite mining process and were provided in dry state Fig. 1 shows a visual comparison of mine tailing with cement, fly ash and silica fume. The mine tailing, in its raw form, is a grey powder and can be denoted by N4 as per Munsell scale; fly ash, cement and silica fume were N4, N5 and 4PB5/3 respectively [34].

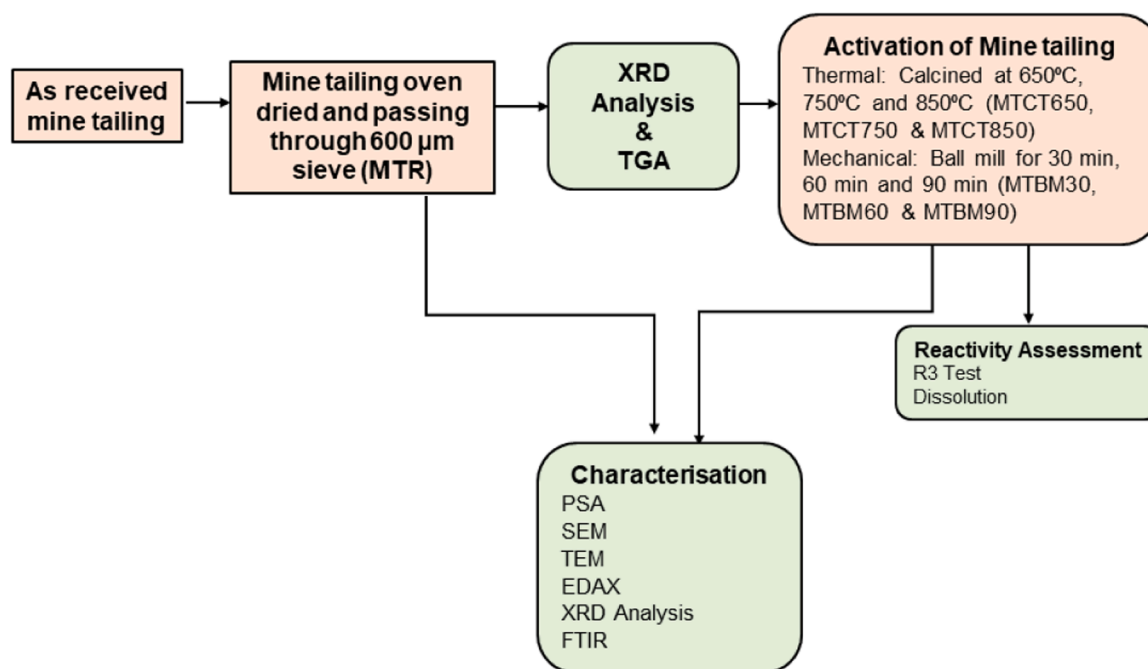


Fig. 2. Experimental methodology flowchart.

## 2.2. Chemicals and reagents

Laboratory grade chemicals and reagents were used in this study. Sodium hydroxide pellets of 98 % extra pure grade from Acros Organics were used to prepare sodium hydroxide solution of required molarity using deionized water for dissolution studies. Potassium hydroxide, of 85 % extra pure flakes, calcium hydroxide of 98 % purity, and granular potassium sulphate of 99 % purity from Acros organics were used in anhydrous form for R3 tests along with calcium carbonate precipitate in powder form that was purchased from Fisher.

Concentrated hydrochloric acid of specific gravity 1.18 and concentration 37 % from Fisher scientific was used for pH adjustment of leachate for dissolution studies. Concentrated HCl was diluted using deionized water to prepare a 1 M HCl solution. Isopropyl alcohol was used for dispersion and cleaning to avoid contamination during analytical studies (SEM, TEM, ICP, XRD). Commercially available fly ash and silica fume were used for benchmarking purposes. The Si and Al standard solution of concentration 1000 mg/mL in HNO<sub>3</sub> from Reagecon was used for calibration of the instrument in dissolution studies. Anatase from Thermo scientific of purity 98 + % was used as an internal standard to quantify the amorphous phase present in mine tailing using Rietveld analysis.

## 3. Experimental methodology

The selection of the activation methods and the associated parameters was done following the identification of the mineral phases present in the mine tailing. The treated tailings were then characterized and compared with the characteristics of raw mine tailing (MTR) to understand the change in properties following activation.

The raw tailing was oven dried at 80°C for 24 h and sieved through a 600 µm sieve to avoid any lumps and achieve sample uniformity. The oven-dried sample was stored in airtight containers in a vacuum chamber and used for further tests that are described in Sections 3.1 to 3.6. For tests which required finer samples, the powders were further crushed and material passing through a 150 µm sieve were used. The summary of the experimental methodology reported here is shown in Fig. 2.

In the initial stage the X ray diffraction analysis and thermo

gravimetry analysis were performed on raw mine tailings. Based on the mineral characteristics different activation methods were employed. The research entailed analysis and comparison of the characteristics of untreated mine tailings and treated mine tailings based on particle size analysis, microstructural analysis, mineralogy, X ray fluorescence analysis, Fourier Transformation Infrared Spectroscopy, x ray diffraction analysis and thermogravimetric analysis, and reactivity assessment tests such as dissolution and adapted rapid, relevant and reliable pozzolanic reactivity test (adapted R3 test). The protocols followed for the tests are discussed in Sections 3.1 to 3.6:

### 3.1. PSA-particle size analysis

The particle size distribution of the raw and ball-milled samples was determined using a laser particle size and particle distribution instrument (HELOS/KF) with RODOS dry dispersion. In this study, the R5 lens was used, covering the size range between 0.5 – 875 µm.

### 3.2. Microstructural analysis and mineralogy

#### 3.2.1. SEM-scanning electron microscopy

Morphology observations of the samples before and after thermal and mechanical activation were conducted using a scanning electron microscope (SEM) (JSM-5700F, JEOL) operated at 20 kV. The samples were secured on carbon tape and sputter coated with gold. Energy dispersive X-ray microanalysis (EDAX) was also performed to identify the elements present. An acceleration voltage of 20 kV was adopted to get a clear image based on trials. An average of two obtained spot values are reported in this study.

#### 3.2.2. TEM-transmission electron microscopy

Transmission electron microscopy (TEM) was performed at 200 kV using a JEOL JEM-1400F for observations of physical and morphological changes in the individual particles with the applied treatment. Isopropyl alcohol was added to 1 g of mine tailing sample in a test tube till it formed a colourless suspension. This suspension was subjected to ultrasonication for 1 minute at a frequency of 20 kHz. A drop of this dispersed sample was mounted on a holey carbon grid using a micropipette. The grid was allowed to dry in a drying chamber at 27 °C for 3 h

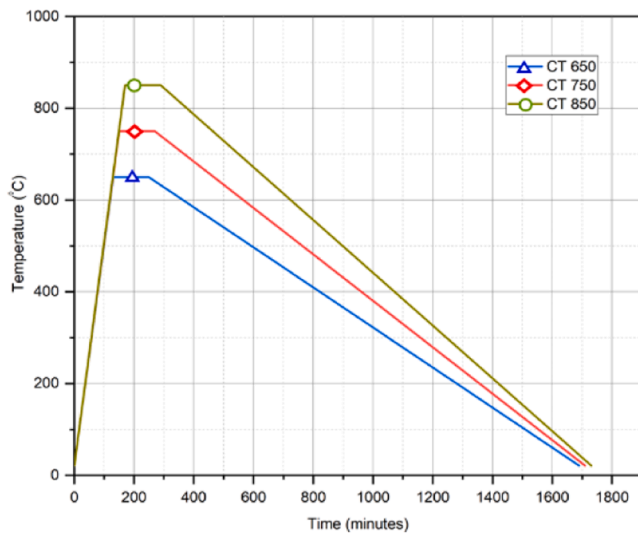
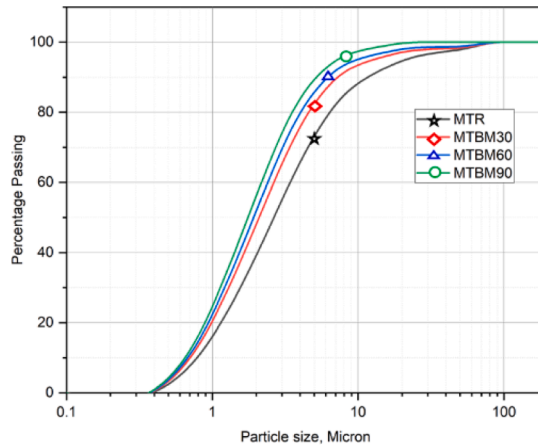
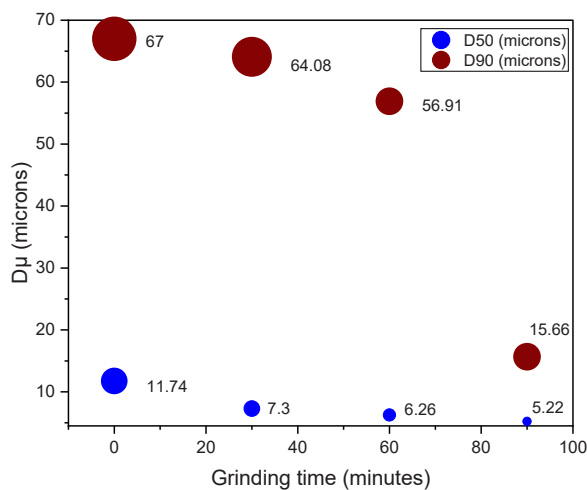


Fig. 3. Heat treatment adopted in the study (CT650, 750 and 850 indicates for calcined at the temperatures 650°C, 750 °C and 850 °C respectively).



(a)



(b)

Fig. 4. Particle size analysis: (a) Particle size distribution of samples before and after milling; (b) Decrease in  $D_{90}$  and  $D_{50}$  values with increase in milling time.

allowing the isopropyl alcohol to evaporate completely.

### 3.2.3. XRF - X-ray fluorescence analysis

The oxide composition of the mine tailing was determined using Panalytical Zetium WDXRF (Wavelength Dispersive X-ray Fluorescence) operated using Panalytical SuperQ software. The data was calibrated WROXI (wide-ranging oxides) standard to determine the oxide concentration in weight %.

### 3.2.4. XRD - X-ray diffraction analysis

X-ray diffraction was performed using a Bruker D8 Advance X-ray diffractometer (XRD), with Cu-K $\alpha$  radiation of wavelength 1.54 Å and radiation energy of 8.04 keV to study the mineralogy. The XRD analysis for performed for a 2 $\theta$  value ranging between 5° and 80°, at a speed of 0.01 ° / step and 1 sec/ step for characterization of raw and activated mineral waste samples. Prior to measurements, mine tailing samples were passed through a 150  $\mu$ m sieve. The fine powder was spread on the sample holder and a glass plate was used to remove the excess material and achieve a flat and smooth surface. The smooth surface ensured that there are no preferred orientation and eliminates any variations in intensity arising because of it. HighScore Plus X-ray diffraction software was used for the analysis of the XRD results [27]. Rietveld analysis was performed using Anatase as an internal standard. 1 g Anatase was uniformly mixed with 9 g of test sample. Rietveld analysis was performed on this sample and the phase quantities were obtained. The resulting composition was normalised to 100 %, giving the absolute composition of individual crystalline phases. The quantities of the individual phases in the actual sample were calculated from the known quantities of Anatase in the crystalline composition and total composition of the material.

### 3.2.5. FTIR - fourier transform infrared spectroscopy

FTIR studies were performed to identify the phase composition and functional groups using a Shimadzu IRSPIRIT ATR Infra-red spectrometer instrument. Mine tailing passing through the 150  $\mu$ m sieve was used for the tests. A micro spatula was used to place the powder sample on the ATR crystal, a diamond surface in this case. Measures were implemented to ensure a consistent pressure was maintained between the press and the crystal for all the samples. For each sample, 16 scans were taken between 4000  $\text{cm}^{-1}$  and 600  $\text{cm}^{-1}$  using the LabSolutions IR Spectrum software.

## 3.3. Thermogravimetric analysis

The mine tailing samples passing the 600  $\mu$ m sieve were investigated using TGA 8000 thermogravimetric analyser by Perkin Elmer in nitrogen environment between 50 °C and 1100 °C and the evolved gases were continuously analysed using Spectrum Two FT-IR Spectrometer (LiTaO<sub>3</sub> Detector). For each sample, 4 scans were taken between 4000  $\text{cm}^{-1}$  and 600  $\text{cm}^{-1}$  using the LabSolutions IR Spectrum software.

## 3.4. Activation of tailings

### 3.4.1. Mechanical activation

Milling of materials in this study serves the purpose of size reduction and mechanical activation of materials. The milling was carried out in a Fritsch Pulversiette 6 planetary ball mill. The XRD analysis of the raw mine tailing indicated the presence of minerals of hardness 2–7 in the Mohs hardness scale. Indicatively, diamond's hardness is a 10 on the Mohs scale while calcite is at 3. Therefore, balls and jar made of tungsten carbide of hardness 9 at the Mohs scale were used for grinding; to prevent wear and tear of the balls and jar, and subsequent contamination of the material. Milling times of 30 min (MTBM30), 60 min (MTBM60) and 90 min (MTBM90) were adopted following observations reported in the literature [33], where 20 min of milling led to reduction of the integral intensity of crystalline peaks and after 80 min of milling there was

**Table 1**

Oxide composition of graphite mine tailing used in the present study in comparison with oxide composition of graphite mine tailing, fly ash, silica fume, GGBFS and cement.

Oxides	As-received mine tailing	Graphite mine tailing [22,43,45]	Fly ash [49]	Silica Fume [49]	GGBS [49]	Cement [50]
SiO <sub>2</sub>	58.46	59.24–64.50	48.20–51.90	94.00–98.00	33.00–37.00	19.30
Al <sub>2</sub> O <sub>3</sub>	14.56	10.21 – 15.05	26.00–30.10	0.10–0.40	8.00–35.00	3.70
Fe <sub>2</sub> O <sub>3</sub>	9.72	5.07–5.80	5.50–11.30	0.02–0.15	0.50–2.00	4.10
Na <sub>2</sub> O	4.36		1.00–3.70	0.10–0.40		0.28
MgO	5.91	1.82 – 3.91		0.30–0.90	6.00–14.00	2.10
K <sub>2</sub> O	2.31	2.26		0.20–0.70		0.88
CaO	2.43	0.84–15.55	2.10–4.20	0.08–0.30	34.00–43.00	63.20
SO <sub>3</sub>	0.27		0–0.10		0.80–2.00	4.00
TiO <sub>2</sub>	1.08					0.29
BaO	0.43					
Mn <sub>3</sub> O <sub>4</sub>	0.02				0.30–1.10	
V <sub>2</sub> O <sub>5</sub>	0.05	0.31				
ZnO	0.06					
ZrO <sub>2</sub>	0.03					
Cr <sub>2</sub> O <sub>3</sub>	0.05					
CuO	0.03					
NiO	0.03					
P <sub>2</sub> O <sub>5</sub>	0.19	0.16				0.17
PbO	0.02					

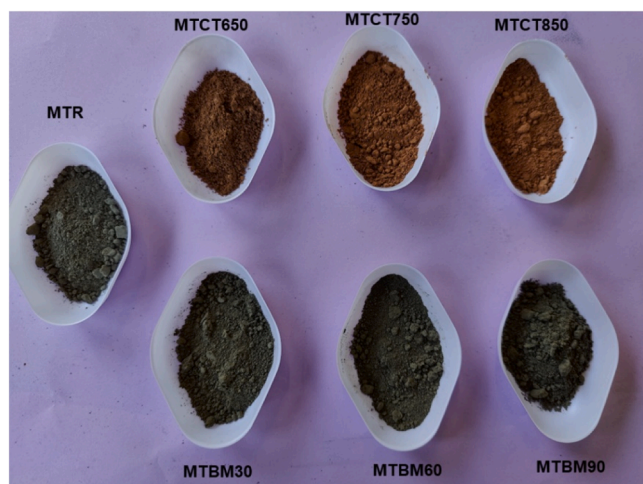


Fig. 5. Appearance of mine tailings before and after activation.

reduction in crystallinity of quartz, albite (plagioclase) and muscovite. The kinetic energy imparted during milling is directly proportional to the diameter of the balls raised to the power four [35]. As the maximum particle size of the material used for grinding is expected to be less than 600  $\mu\text{m}$  after sieving, a maximum suitable size of 10 mm balls was used, to optimize the diameter and the imparted collision energy (kinetic energy) [35].

### 3.4.2. Thermal activation

The calcination temperatures were determined based on the mineralogy and recommendations from existing literature. As the initial XRD indicated presence of kaolinite and phlogopite, the calcination temperatures above 650°C were chosen. Published work [36] suggests that heating above 900°C leads to formation of new crystalline aluminosilicate mineral phases which may reduce the reactivity of the activated tailing. Therefore, calcination temperatures of 650°C, 750 °C and 850 °C were adopted and the samples calcined at this temperature are designated MTCT650, MTCT750 and MTCT850, respectively.

A ramp up rate of 300°C/ hour was used to comply with the thermal expansion of the crucible and prevent fracture due to thermal shock. The samples remained at the set temperature for 2 h to ensure complete calcination. The sample was allowed to cool gradually in the furnace to

avoid thermal shock due to sudden exposure to the atmosphere and removed when it reached room temperature. The entire calcination cycle is as shown in Fig. 3. A tray-shaped fused alumina crucible (of internal dimensions 217x95x60 mm and a wall thickness of 16 mm) was used for this purpose. To ensure uniform heating of the sample the powders were evenly spread in the crucible to a height of 15 mm.

### 3.5. Dissolution of Si and Al

The Solubility of Si and Al in NaOH are good indicators of the availability of Si and Al within an alkali activated system for condensation and gel formation [37,38]. By identifying, the solubility of Si and Al, conclusions can be drawn as to whether the activated tailing can be utilized to produce alkali-activated binders.

The solubility tests were carried out using 8 M NaOH. The NaOH solution was prepared in advance and allowed to cool down to room temperature. The solution was prepared in batches of 2 L. And a temperature setting of 23°C and a mixing speed of 200 rpm was adopted. For each 1 g oven-dried material passing through the 150  $\mu\text{m}$  sieve, 50 g NaOH solution was added and mixed using a magnetic stirrer for 6 h at 23°C and a mixing speed of 200 rpm. The solution was filtered through a 0.45  $\mu\text{m}$  pore size filter. The leachate was diluted using deionized water at 1:50 ratio. This diluted leachate was acidified to a pH of 2 to prevent settling of the ions by slow addition of 1 M HCl using a pipette. An Inductive Coupled Plasma Optical Emission Spectrometer (ICP-OES) fitted with a sea spray nebulizer and SPS3 autosampler was used for determining Si and Al that leached into the alkaline solution from the mineral waste.

### 3.6. Pozzolanic activity

The assessment of the chemical reactivity (pozzolanicity) of the treated tailings within a simulated cementitious matrix was performed following the provisions of rapid, relevant and reliable pozzolan reactivity test - R3 test, (ASTM C1897(2020)) but at modified temperature (60 °C instead of 40 °C). Due to the low reactivity observed in the MTR samples, the heat of hydration for these samples in R3 test were rather low when the test was performed at 40 °C, this resulted in heat flow values indistinguishable from system noise. It has been reported [39] that the latent hydraulic reaction and pozzolan reactions in presence of calcium hydroxide can be activated by increase in temperature. Therefore, the test temperature was increased from 40 °C to 60 °C consequently, enhancing the reactivity for non- reactive and less

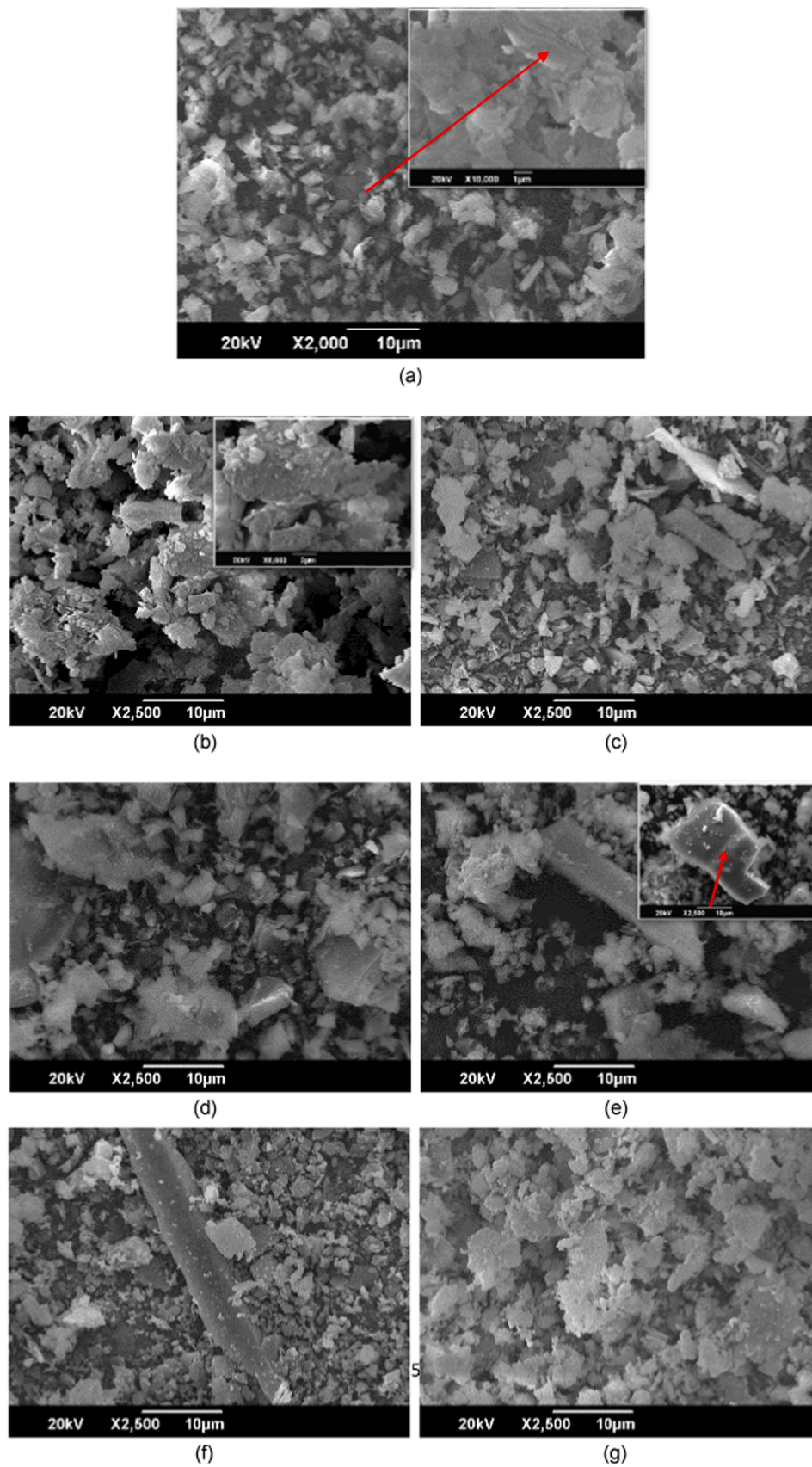


**Fig. 6.** SEM images of samples used in this study: (a) MTR, Inner image – Sheet-like appearance of phyllosilicates in MTR samples. Red arrow points at the layered appearance of phyllosilicates; (b) MTCT650 shows appearance of flocculant particles; (c) MTCT750; (d) MTCT850; (e) MTBM30, inner image - SEM image showing the development of cracks in particles of MTBM30; (f) MTBM60; and (g) MTBM90. Note: CT refers to calcined tailings and BM refers to ball milled tailings.

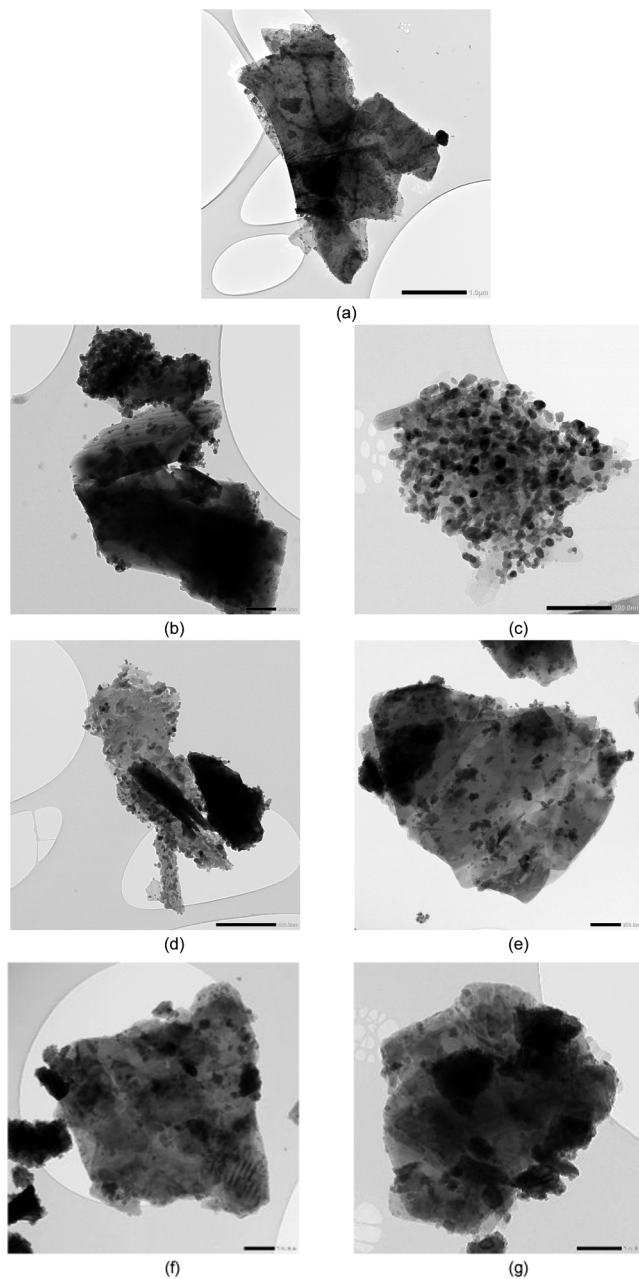


**Fig. 7.** TEM images of untreated and processed mine tailing samples. (a) MTR particle shows crystalline characteristics and is angular; (b) MTCT650 shows beginning of sintering and aggregation in particles; (c) MTCT750 particles exhibiting aggregation and sinter necks; (d) MTCT850; (e) MTBM30 particles showing softened edges after milling; (f) MTBM60; (g) MTBM90 particles with rounded edges after milling. Note: CT refers to calcined tailings and BM refers to ball milled tailings.

reactive materials [39]. Nevertheless, it is crucial to take into account that performing the test at an elevated temperature renders the results not comparable to the typically performed R3 test values and also results in a reduction in the recorded heat of hydration [39].

The experimental procedure involved producing a mix containing 10 g mineral waste, 30 g calcium hydroxide, 5 g calcium carbonate and 54 g potassium solution. The potassium solution contains 4.00 g/L potassium hydroxide and 20.0 g/L of potassium sulphate dissolved in deionised water. The heat of hydration of this mix was monitored, using an I-Cal HPC - High Performance Calorimeter, for a period of 7 days under the constant temperature of 60 °C. The first 75 min of the tests were not taken into consideration due to temperature differences as

recommended [40–42]. Cumulative heat, at the end of three and seven days, per gram of material was reported. The higher heat of hydration indicates a higher degree of reactivity.

To minimize the difference in temperature all the materials and the containers used were conditioned at 60 °C for 24 h prior to the start of the procedure. In addition to the tailing samples, for benchmarking purposes the R3 test was performed for silica fume and fly ash which are known for their reactivity in cementitious systems.

## 4. Results and discussions

### 4.1. Particle size distribution

The mine tailing used in this study was fine in its raw form, with 99 % of the particles finer than 67.00 μm which was further reduced to 15.66 μm after 90 min of milling. The particle size distribution as shown in Fig. 4a indicates a uniform size distribution of the samples and the gradual reduction in particle size after milling for 30 min (MTBM30), 60 min (MTBM60) and 90 min (MTBM90). The reduction in  $D_{50}$  and  $D_{90}$  values with milling is given in Fig. 4b. The median particle sizes ( $D_{50}$ ) were reduced by 37.82 %, 46.67 % and 55.54 % from the initial particle size after 30, 60 and 90 min of milling respectively, whereas for  $D_{90}$  the reductions were 4.36 %, 15.06 % and 76.62 % respectively. This indicated that the longer duration of milling is more effective for reducing the particle size of coarser particles and did not have a significant effect on the finer particles. However, further milling would have led to the aggregation of finer particles, and thus affecting the reactivity negatively.

### 4.2. Chemical composition, microstructure, and mineralogy

Table 1 shows the chemical composition of the as-received mine tailing. It is evident that silicon dioxide has a dominant presence in the material, something that is in agreement with other graphite tailings mentioned in the literature [43–45]. While the high concentration of  $\text{SiO}_2$  that exists in silica fume cannot be easily matched, the mine tailing with about 58.50 %  $\text{SiO}_2$  content is very comparable to commercially available fly ash.

Other major oxides include alumina and ferric oxide with 14.60 % and 9.70 % respectively. Oxides of sodium, magnesium, potassium, and calcium were also present in the range of 2.3–5.9 %.

The modulus of hydraulicity ( $M_h$ ) as determined by Eq. (1) assesses the ability of a material to undergo hardening through the formation of reaction products upon contact with water [46,47]. The strength activity index is reported to increase with increase in modulus of hydraulicity [47]. The  $M_h$  value of MTR is 0.03.

$$M_h = \frac{\text{CaO}}{\text{Fe}_2\text{O}_3 + \text{SiO}_2 + \text{Al}_2\text{O}_3} \quad (1)$$

Similarly, the modulus of basicity/ basicity coefficient ( $M_b$ ) [48] determined by Eq. 2 is 0.11 for MTR.

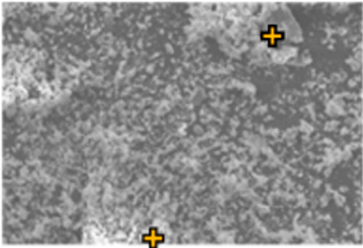
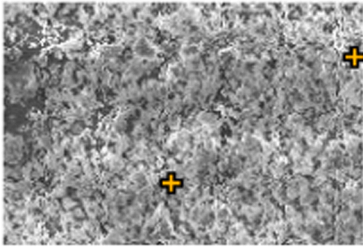
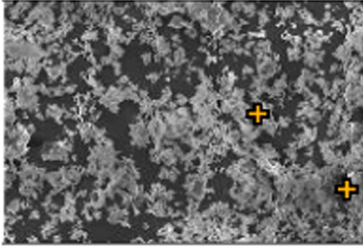
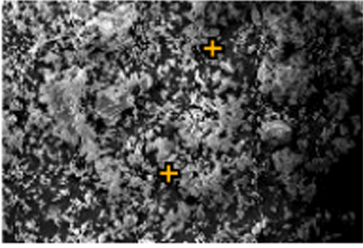
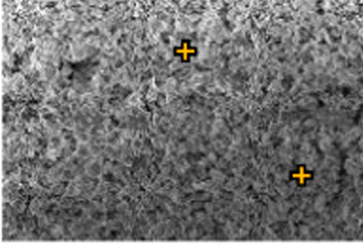
$$M_b = \frac{\text{CaO} + \text{MgO}}{\text{SiO}_2 + \text{Al}_2\text{O}_3} \quad (2)$$

The recommended range for modulus of basicity is between 0.70 – 1.20 [48] for the material to be suitable for alkali activation. This gives an indication on whether the chosen material is suitable for alkali activation without use of an alternative/ additional source for silica or alumina, especially in case of amorphous precursors such as fly ash and ground granulated blast furnace slag. Nevertheless, the computed values of basicity modulus and hydraulicity modulus for MTR do not accurately represent the reactivity of this material. This is because these ratios are developed to estimate the reactivity of amorphous materials. Therefore, they do not consider the proportion of ions that are readily available for reaction, as well as the presence of non-reactive ions in crystalline form as observed in case of a highly crystalline material.

The visual observation indicated that MTR samples were grey in colour [34] and calcined samples turned to brick red colour due to oxidation of Fe present in the mine tailing to  $\text{Fe}_2\text{O}_3$  as shown in Fig. 5. Of these MTCT750 and MTCT850 had a brighter red hue when compared to MTCT650. This indicates that the samples calcined at and above 750°C, are oxidized completely.

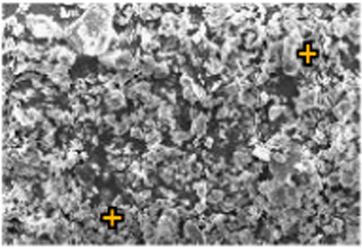
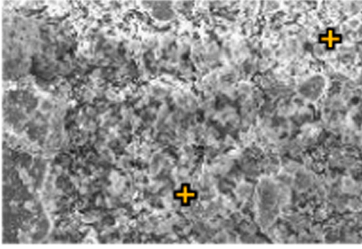
The microstructure of samples observed by SEM is given in Fig.6 (a) to (g). The MTR samples (Fig. 6 (a)) were highly crystalline with dense particles of size ranging from about 1  $\mu\text{m}$  to 70  $\mu\text{m}$ . The particles were angular with sharp edges and with an uneven particle size distribution. The smaller particles were found to adhere to the surface of the larger particles. The observations were similar to those made by Yu et al. [51]

**Table 2**  
Elemental Composition of MT.

Sample ID	Image	Elemental composition
MTR		<b>Element</b>
		O
		Na
		Mg
		Al
		Si
		S
		K
		Ca
		Fe
MTCT650		<b>Element</b>
		O
		Na
		Mg
		Al
		Si
		S
		K
		Ca
		Fe
MTCT750		<b>Element</b>
		O
		Na
		Mg
		Al
		Si
		S
		K
		Ca
		Fe
MTCT850		<b>Element</b>
		O
		Na
		Mg
		Al
		Si
		S
		K
		Ca
		Fe
MTBM30		<b>Element</b>
		O
		Na
		Mg
		Al
		Si
		S
		K
		Ca
		Fe

(continued on next page)

Table 2 (continued)

Sample ID	Image	Elemental composition		
MTBM60		<b>Element</b>	<b>Weight (%)</b>	<b>Atom (%)</b>
		O	36.22	52.24
		Na	3.06	3.08
		Mg	3.62	3.44
		Al	8.30	7.10
		Si	31.16	25.60
		S	1.93	1.39
		K	2.05	1.21
Ca	1.83	1.06		
Fe	11.85	4.91		
MTBM90		<b>Element</b>	<b>Weight (%)</b>	<b>Atom (%)</b>
		O	34.30	50.71
		Na	2.44	2.52
		Mg	4.90	4.76
		Al	8.30	7.28
		Si	29.43	24.81
		S	1.22	0.90
		K	3.15	1.90
Ca	1.50	0.89		
Fe	14.79	6.27		

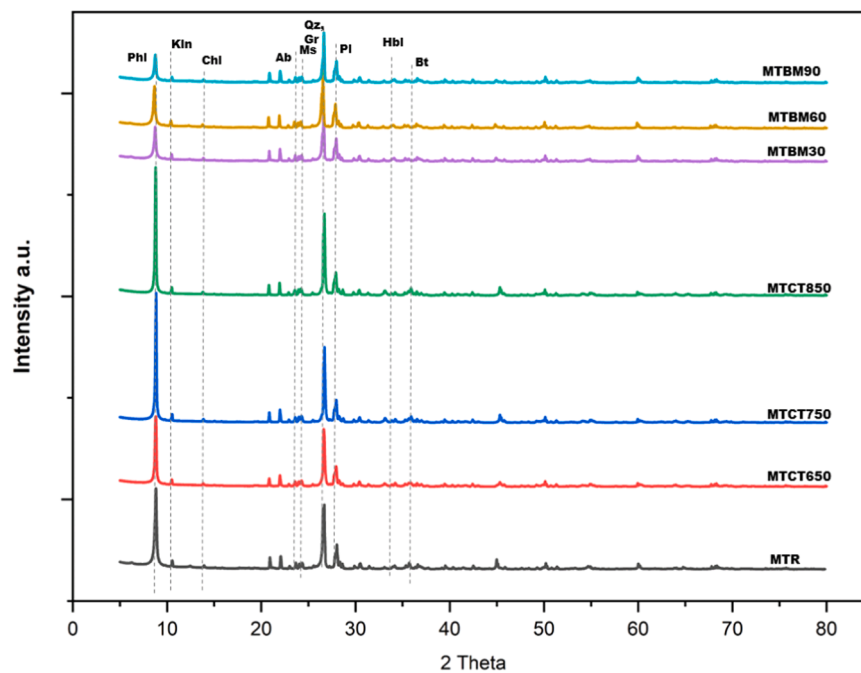


Fig. 8. XRD phases of mine tailing samples before and after activation. Phl – Phlogopite, Kln – Kaolinite, Chl – Chlorite, Ab – Albite, Ms – Muscovite, Gr – Graphite, Qr – Quartz, Pl – Plagioclase, Hbl – Hornblende, Bt – Biotite. Note: CT refers to calcined tailings and BM refers to ball milled tailings.

and Ren et al. [52]. Wu et al. [24] suggested that this particle agglomeration of mine tailing can negatively influence the rheology of mine tailing-based cements.

On a higher magnification as shown in Fig. 6a (inner image), sheet-like layers observed indicating phyllosilicate crystals are observed in MTR [53]. Fig. 6b to d are images of calcined tailing. The calcination process results in the formation of particles of flocculant appearance as shown in Fig. 6b (inner image). Similar changes were observed by Yu et al. [51]. Fig. 6c and d show partial vitrification and melting which indicate that further heating could lead to the fusing and melting of certain phases as reported by Luo et al. [54].

The sample after milling had more small sized particles of size less

than 5  $\mu\text{m}$  (Fig. 6e to g) and the large sized particles (25  $\mu\text{m}$  or larger) appeared to have cracks as shown in Fig. 6e and f. No agglomeration of samples was observed until 90 min of milling. The presence of fewer large sized particles and more smaller size particles can be attributed to a phenomenon called selective grinding. Here the minerals of higher hardness had a larger particle size, and the minerals of lower hardness had a better particle size reduction for the same milling energy [55]. This is also in agreement with the observations made from particle size analysis where the  $D_{90}$  of the particles was about 5.70 times that of  $D_{50}$  before milling, whereas that value was 8.80 times  $D_{50}$  after 30 min of milling. This indicates that the initial milling had an effect on particles of lesser hardness and not on the ones with higher hardness leading to

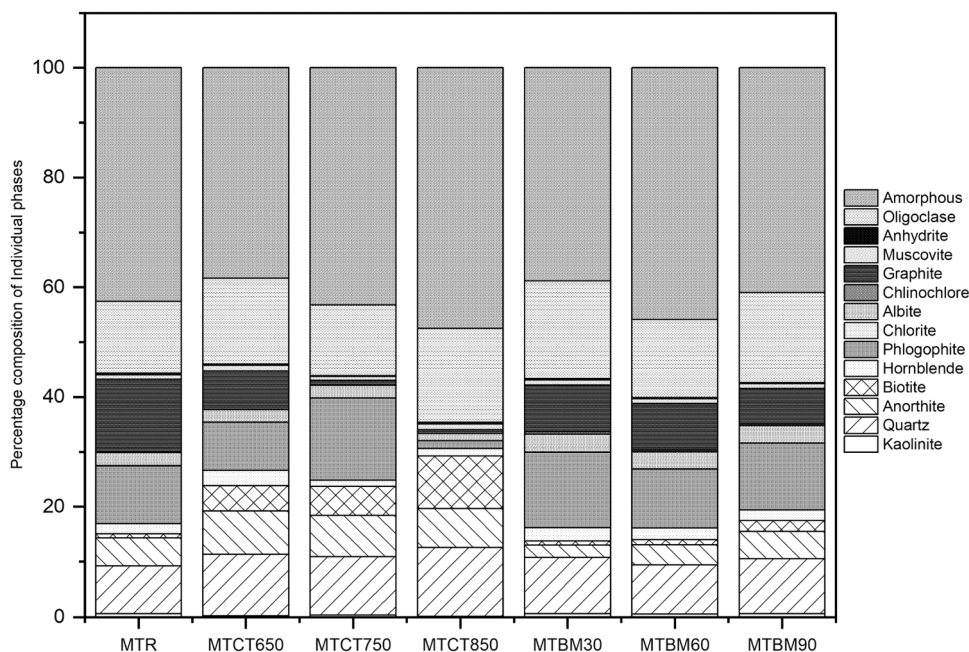


Fig. 9. Mineral Phases and their respective % composition. Note: CT refers to calcined tailings and BM refers to ball milled tailings.

Table 3  
Mineral phases in mine tailing and their respective percentages.

Mineral phases	MTR	MTCT650	MTCT750	MTCT850	MTBM30	MTBM60	MTBM90
Kaolinite	0.64	0.25	0.34	0.11	0.61	0.54	0.59
Quartz	8.55	11.05	10.51	12.42	10.12	8.81	9.88
Anorthite	5.09	7.90	7.56	7.11	2.27	3.68	5.03
Biotite	0.75	4.63	5.28	9.58	0.74	0.97	1.95
Hornblende	1.85	2.78	1.14	1.37	2.39	2.11	1.95
Phlogopite	10.52	8.77	15.00	1.47	13.80	10.76	12.19
Chlorite	0.12	0.00	0.00	0.00	0.00	0.00	0.00
Albite	2.31	2.35	2.27	1.26	3.25	3.08	3.20
Clinocllore	0.12	0.00	0.00	0.00	0.43	0.32	0.30
Graphite	13.29	6.98	0.91	0.68	8.53	8.54	6.45
Muscovite	0.81	1.11	0.74	1.05	0.98	0.86	0.89
Anhydrite	0.29	0.19	0.11	0.32	0.25	0.22	0.18
Oligoclase	13.06	15.68	12.90	17.11	17.79	14.22	16.45
Amorphous	42.60	38.33	43.24	47.53	38.83	45.89	40.95

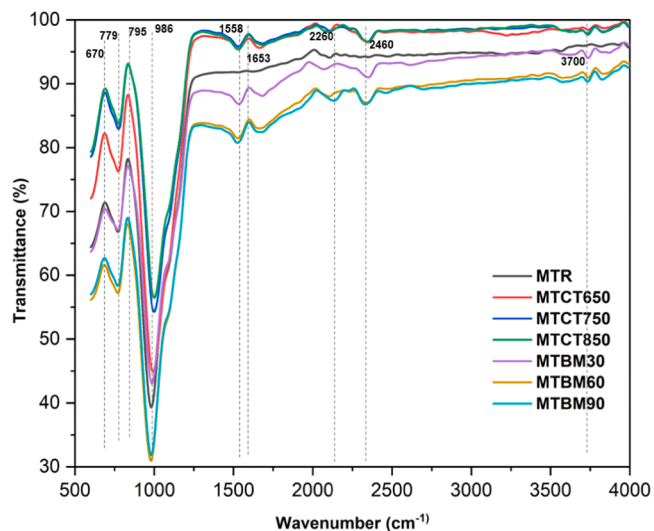


Fig. 10. FTIR spectra of MT before and after activation. Note: CT refers to calcined tailings and BM refers to ball milled tailings.

Table 4  
FTIR absorbance bands and assignments.

Wavelength (cm <sup>-1</sup> )	Assignment	Ref.
667–795	Si-O-Si symmetrical stretching	[64,65]
950–1200	Asymmetric stretching of Al-O and Si-O	[58–60]
1600–1700	Bending vibration H-O-H	[60]
2200–3600	Stretching of O-H	[59,60]

significant change in the difference between D<sub>50</sub> and D<sub>90</sub>.

Individual crystals were also observed using TEM (Fig. 7a to g). The primary particle observation indicated that the mine tailing particles were polycrystalline. The mine tailing particles had sharp angular edges. Though the mine tailing particles appeared crystalline after calcination at 650°C and 750°C, some particles exhibited signs of aggregation and sinter necks at 750°C as shown in Fig. 7(b), (c) and (d). This could be due to the primary crystallites forming solid bridges during the calcination process [56]. However, it is evident that with increasing temperatures the morphology of the particles changes. The originally solid angular MTR crystals gradually change to an amorphous material.

The EDAX analysis of samples given in Table 2 has confirmed that the as-received tailing is predominantly in the form of silicate with high

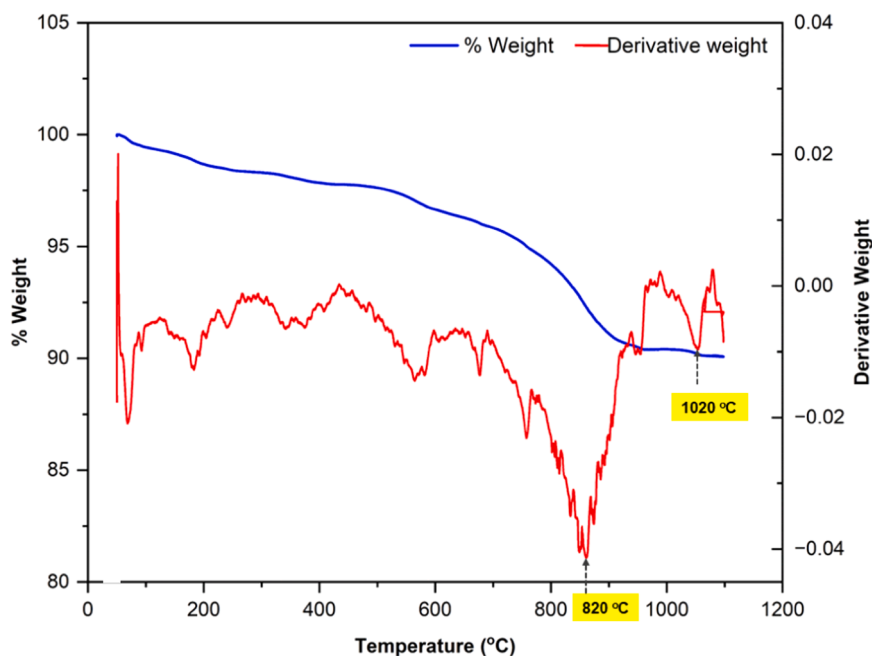


Fig. 11. TGA analysis of the MTR.

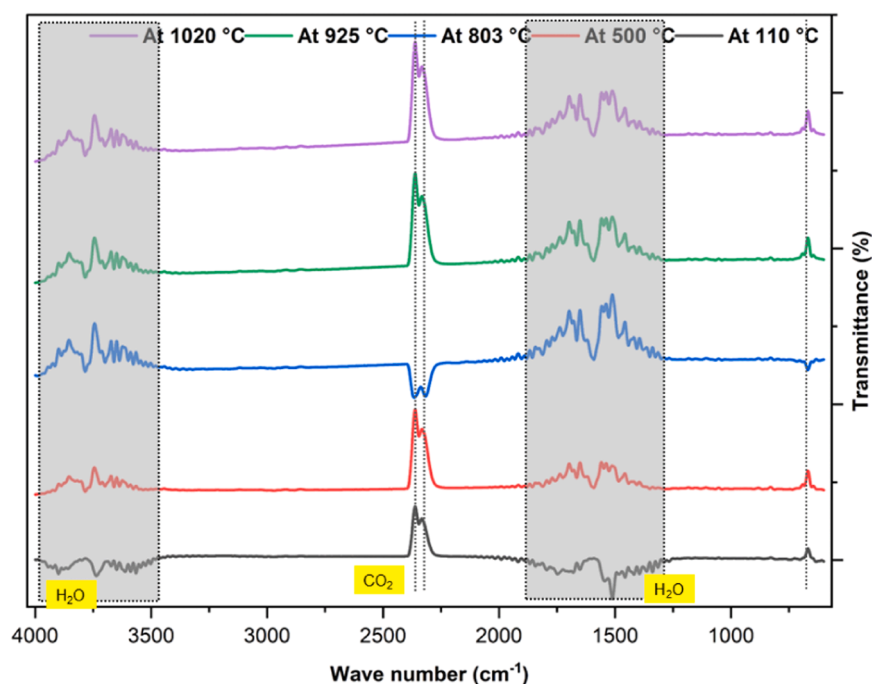


Fig. 12. FTIR analysis of gases evolved during TG analysis.

amounts of alumina. The high amounts of silicate and alumina are not typically affected by any of the treatment methods adopted in the study.

The XRD diffractograms (Fig. 8) indicated that the mine tailing was highly crystalline. The mineral phases identified from Fig. 8 and their corresponding COD reference ID are as follows: Chlorite (96-900-4189), Clinocllore (96-901-0130), Kaolinite (96-155-0599), Muscovite (96-901-5624), Phlogopite (96-900-2830), Biotite (96-900-0468), Quartz (96-50-0036), Hornblende (96-900-1245), Graphite (96-901-2231), Anhydrite (96-500-0041) and Plagioclase minerals such as Oligoclase (96-901-1423), Anorthite (96-900-0362) and Albite (96-900-9664), are the mineral phases present in MTR and

no new phases were observed in the activated mine tailing. In order to enhance the comprehensibility of the X-ray diffraction (XRD) patterns, certain subgroup minerals, such as clinocllore, are annotated with the corresponding parent group to which they belong, such as chlorite. Similarly, oligoclase and anorthite are marked as plagioclase. The quantities of various phases present are given in Fig. 9 and Table 3. It can be observed that the MTR was 42.60 % amorphous and the treated mine tailings were in the range of 38.33–47.52 % amorphous. However, it is to be noted that about 4.75 % - 12.38 % of the crystalline phase constituted by graphite disappears due to calcination/ heat generated during mechanical activation. This phase will be converted to carbon

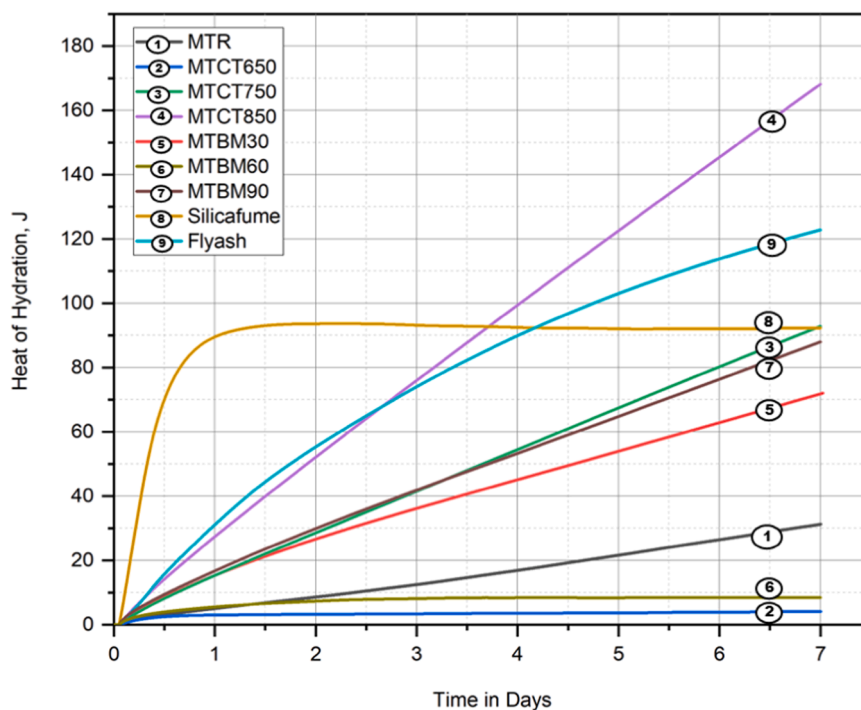


Fig. 13. Heat of hydration from R3 test of MT at 60 °C. Note: CT refers to calcined tailings and BM refers to ball milled tailings.

dioxide and will not contribute to amorphous phase quantities or crystalline phase quantities. This reduction in the total quantity of the material might contribute to the seemingly increased quantities of phases such as biotite, quartz and phlogopite at calcination temperatures 650 °C and 750 °C. The decomposition of phlogopite begins at 800 °C and this leads to a decrease in the quantity of phlogopite at 850 °C.

FTIR spectra of the mine tailing before and after activation are given in Fig. 10 and peak assignments based on literature are given in Table 4. The peaks at  $779\text{ cm}^{-1}$  and  $795\text{ cm}^{-1}$  correspond to Quartz and these peaks remain without any significant alteration after activation [57]. The major peak occurs at around  $986\text{ cm}^{-1}$ , which is in general attributed to asymmetric stretching of Si-O and Al-O [58–60]. These peaks were also observed to shift slightly towards the higher wave number. The observed phenomenon can be attributed to the alterations in the structural configuration of the Al-O and Si-O chemical bonds within the constituent phases found in tailings. The lower internal order of the bonds in the tailing due to calcination may lead to peak broadening of the entire envelope, which in this case might be attributed to formation of  $Q^0$  silicate tetrahedra species [61]. The observed peaks within the spectral range of  $1900\text{--}2350\text{ cm}^{-1}$  are also indicative of distinct carbon bonds, including C-OH, C-H, CO, C-C, and OH. The alterations in the shape, intensity, and symmetry of these peaks of can also be ascribed to oxidation and chemical interactions occurring within the graphite phase during the calcination processes [62]. The peaks at wavenumbers  $1558\text{ cm}^{-1}$  and  $1653\text{ cm}^{-1}$  are indicative of the bending vibrations of the H-O-H bond. These peaks intensified upon calcination indicating the changes in phases with H-O-H bonds upon calcination. The spectral region spanning from  $3300\text{ to }3750\text{ cm}^{-1}$  which can be associated with the stretching and bending vibrations of O-H bonds exhibits a development of new peaks and intensification of existing peaks. The observed alterations in O-H bonds may be attributed to the variations in the crystal structure and composition of chlorite, biotite, phlogopite, kaolinite and hornblende following the process of calcination [59,60,63]. All these compounds possess O-H bonds and demonstrate changes in their crystal structure upon calcination, as indicated by the XRD patterns and quantitative analysis.

FTIR spectrum of the ball milled samples showed peaks at  $779\text{ cm}^{-1}$  and  $795\text{ cm}^{-1}$  are indicative of the presence of Si-O-Si bonds within the

quartz crystal. The peaks exhibited minimal alterations both prior to and subsequent to the milling process. The peak observed at around  $966\text{ cm}^{-1}$  is widely recognised as being indicative of the asymmetric stretching of Si-O and Al-O bonds that are typically found in the alumino silicate mineral phases present in tailings. A small shift towards the lower wavenumber accompanied by a marginal decrease in intensity of less than 5 % was observed for milled samples. The observed behaviour can be explained by the changes in the structural arrangement of the Al-O and Si-O chemical bonds present in the constituent phases present in tailings. The observed shift in this study can be related to alterations in the Al-O and Si-O bonds of alumino silicate minerals, specifically phlogopite and biotite [59,60,63]. The peak intensity of these minerals notably decreased during the milling process, as indicated by the XRD results.

The TG analysis of the mine tailing given in Fig. 11. The sample exhibits a gradual weight loss between 50 °C and 600 °C. The initial weight loss observed from 50 °C to 400 °C corresponds to loss of physically adsorbed water [66]. The weight loss observed in the region 600 °C - 850 °C correspond to dehydroxylation of kaolinite and decomposition of chlorite. The change in weight between 800 °C to 1050 °C corresponds to the decomposition of chlorite, phlogopite, biotite and clinoptilolite. This observation is also in agreement with the findings of the XRD phase analysis which shows about 86 % reduction in phlogopite, and the disappearance of the chlorite and clinocllore phases. The changes above 1000 °C can be attributed to the beginning of decomposition of phlogopite minerals and the continued decomposition of plagioclase phases such as albite, anorthite and oligoclase.

However, as the TG analysis was performed in an inert environment the graphite phase which might have otherwise been converted to  $\text{CO}_2$  remains inert.

The evolved gas were recorded continuously using FTIR and the gas spectrum at five different temperatures corresponding to changes in TGA curve are reported in Fig. 12. Fig. 12 shows the evolution of traces of  $\text{CO}_2$  and  $\text{H}_2\text{O}$ . Though these gases are emitted at all temperatures the spectrum at 803 °C records a higher transmittance. This is in line with the TGA analysis where the major weight loss is observed at around 800 °C to 900 °C.

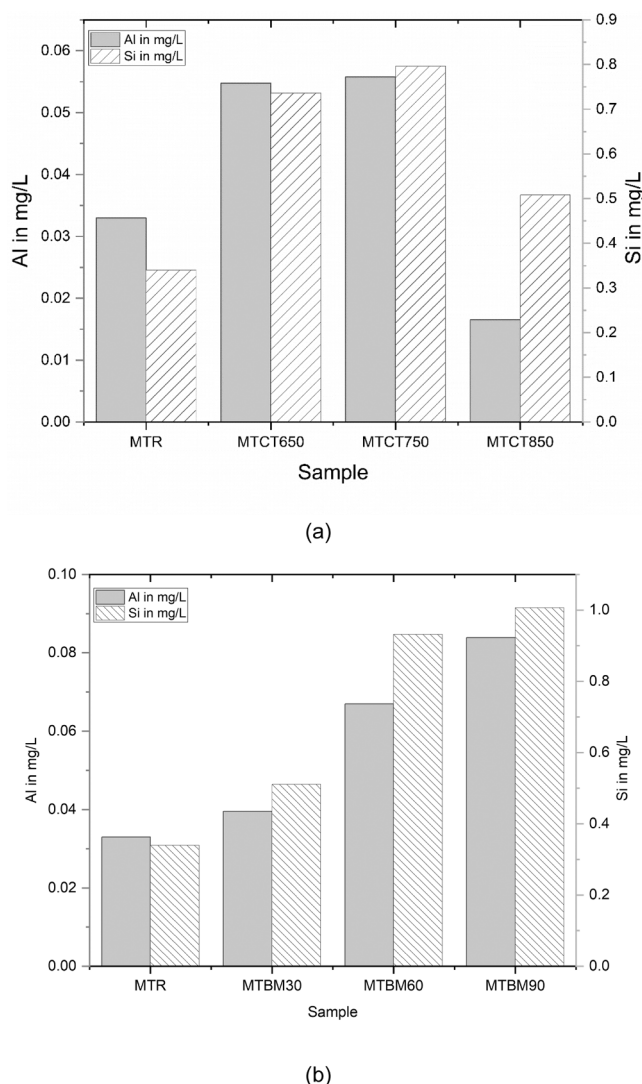


Fig. 14. Solubility of Si and Al from: (a) raw and thermally treated mine tailing and (b) raw and mechanically treated tailing. Both studies performed in 8 M NaOH.

#### 4.3. Chemical reactivity by modified R3 test

The heat of hydration with time is reported in Fig. 13. The data show that the initial high heat of hydration followed by slower or almost no heat of hydration shows a typical trend of a highly reactive supplementary cementitious material as reported in the literature. From Fig. 13, it is evident that the behaviour of silica fume fits this description [39,67].

While MTCT650 samples were found to be almost inert, MTR, MTBM30, MTCT750, and MTCT850 show a trend like that of a slow reactive material [39,68], a trend which is also verified by the behaviour of fly ash. From Fig. 13 it can also be inferred that reactivity of fly ash and MTCT850 was better than that of silica fume at later ages (after 3 days) and MTCT750 was almost equal to that of silica fume at the end of seven days. These findings link very well with previous observations made in this study. It seems that while the calcination at 650 °C does not have any influence on the mine tailing, treatment at 750 °C and 850 °C has yielded a reactive compound that resembles fly ash in terms of pozzolanic behaviour. In the case of MTCT850, the performance of the tailing appears even better than that of fly ash, with heat of hydration about 1.35 times higher compared to fly ash.

Ball-milling seems to have a similar effect for the longest milling

duration, with MTBM90 being very similar to MTCT750.

#### 4.4. Dissolution of Si and Al

The solubility of Si and Al in alkaline environment is obtained from ICP. This gives an indication of the Si and Al available for formation of hydration products in an alkaline environment and hence the value is directly proportional to the reactivity of the material in an alkali activated cement or in a cementitious system [37]. The Si/Al ratio obtained from the test can provide an indication on type of activator that would be suitable if mine tailing is used as a precursor for alkali activation (sodium hydroxide, sodium silicate etc) or if it should be used in combination with an Al rich source (in the form of alumina, red mud, kaolinite etc). The results of the tests (of the diluted leachate) reported in Fig.14(a) and (b), show that samples MTCT650, MTCT750, MTBM60 and MTBM 90 had higher Si and Al in the leachate. It is observed that the percentage of Si and Al in the leachate increased with milling. The amount of Al was 154 % higher and Si was 196 % higher than MTR for MTBM90. In the case of calcination, Al quantity increased 60–66 %, while Si was 116–134 % higher for MTCT650 and MTCT750 than MTR. However, in case of MTCT850 there was an increase of 47 % for Si and decrease of 49 % for Al than MTR. This implies that milling of samples was more effective in improving the dissolution of Si and Al from mine tailings than calcination. This phenomenon can be used to imply that the milled samples are more suitable for alkali activation than the calcined samples.

#### 5. Conclusions

This paper presented characterization studies of raw and activated graphite mine tailing. The findings of the study showed that the tailing used was predominantly silicate. Mineralogical composition of the sample was assessed with X-ray diffraction (XRD). The MTR samples exhibited the presence of various minerals including chlorite, clinocllore, kaolinite, muscovite, phlogopite, biotite, quartz, hornblende, graphite, anhydrite, and plagioclase minerals such as oligoclase, anorthite, and albite. The mineral composition indicated a possibility of activation by calcination and high energy milling. The activated samples when tested had a modified morphology and performance. The Rietveld analysis, Fourier Transform Infrared Spectroscopy (FTIR), determination of elemental composition, and examination of microstructure collectively revealed alterations in the mineral phases and morphology resulting from the treatment processes employed. The reactivity of the activated samples was evaluated by examining their solubility in an alkaline environment using ICP-OES and measuring their heat of hydration using adapted R3 tests. These tests also helped in determining the optimum treatment method. It was determined that tailing calcined at 850°C exhibited a higher heat of hydration and thus shows potential for use as a supplementary cementitious binder. And the samples milled for 90 min exhibited greater concentration of soluble silicon (Si) and aluminium (Al) in sodium hydroxide solution, in comparison to the MTR samples. A property which might prove beneficial in alkali activated cementitious systems.

The aforementioned tests produced findings that both collectively and individually suggest that the treatment processes employed, (i.e.) calcination and ball milling, has resulted in effective alterations to the particle size, morphology, and mineralogy of the material. This demonstrates that the strategy for selection of treatment process for the material based on its mineralogical composition has proven to be successful. The mine tailing, when subjected to suitable treatment, demonstrated promise as a viable component in cementitious binders.

Extensive analysis and tests are needed to find the performance of this material in a cementitious systems. Future study in this topic should encompass not only the technical aspects of mineral waste utilisation but also acknowledge and address the existing constraints and problems that impede the widespread implementation and large-scale valorisation.

Key points to emphasize include the urgent need for a more profound understanding of these materials, the development of appropriate legislation and standards, and addressing environmental concerns related to heavy metal content. Furthermore, collaborative efforts among researchers, industry stakeholders, and regulatory bodies are essential to propel this emerging field forward and establish sustainable practices for mineral waste management and repurposing. This is an emerging area with significant potential, but it requires comprehensive multidisciplinary efforts to overcome existing hurdles and unlock its full benefits for a greener future.

#### CRedit authorship contribution statement

**Chaliasou Napoleana Anna:** Writing – original draft, Supervision, Methodology, Investigation. **Akram Sufyan:** Writing – original draft, Methodology, Investigation. **Chrysanthou Andreas:** Writing – review & editing, Writing – original draft, Supervision, Resources, Methodology, Investigation. **Kanellopoulos Antonios:** Writing – review & editing, Writing – original draft, Supervision, Project administration, Methodology, Investigation, Conceptualization. **Maruthupandian Surya:** Writing – review & editing, Writing – original draft, Methodology, Investigation, Formal analysis, Conceptualization.

#### Declaration of Competing Interest

The authors declare that they have no known competing financial interests or personal relationships that could have appeared to influence the work reported in this paper.

#### Acknowledgements

This project has received funding from the European Union's Horizon 2020 research and innovation programme under the Marie-Sklodowska-Curie grant agreement No - 801604. The authors would like also to express their gratitude to Dr Theodore Hanein and Dr Aniruddha Baral of the University of Sheffield, for their help with the XRF data.

#### Data availability

Data will be made available on request.

#### References

- [1] A.C. Ferguson, P. Griffin, E. Amadi, O. Weber, J. Rouvillois, Net Zero: In a Binder, n.d.
- [2] International Energy Agency, Technology Roadmap - Low carbon Transition in the Cement Industry Foldout, 2018. <https://doi.org/10.1007/springerreference.7300>.
- [3] CEMBUREAU, Cementing the European green deal, n.d.
- [4] A. Mullholland, C. Ackerman, P. Astle, M. Drowniok, A. Dunster, A. Hibbert, R. Inman, R. Kershaw, B. Martin, C. McCague, C. Price, G. Thompson, Low Carbon Concr. Route (2022). (<https://www.ice.org.uk/events/latest-events/low-carbon-concrete-routemap-launch>).
- [5] J.S. Adiansyah, M. Rosano, S. Vink, G. Keir, A framework for a sustainable approach to mine tailings management: Disposal strategies, J. Clean. Prod. 108 (2015) 1050–1062, <https://doi.org/10.1016/j.jclepro.2015.07.139>.
- [6] R. Obenaus-Emler, M. Falah, M. Illikainen, Assessment of mine tailings as precursors for alkali-activated materials for on-site applications, Constr. Build. Mater. 246 (2020) 118470, <https://doi.org/10.1016/j.conbuildmat.2020.118470>.
- [7] L. de Carvalho Medeiros, M.S. de Moura, L.F.S. Fernandes, A.M. da Costa, F.A. L. Pacheco, The economic valuation of environmental damages in scenarios of tailings dams' ruptures: the case of Brumadinho's catastrophe, Minas Gerais, Brazil, Case Stud. Chem. Environ. Eng. 11 (2025), <https://doi.org/10.1016/j.cscee.2024.101037>.
- [8] C. Reichl, M. Schatz, World Mining Data 2021, Federal Ministry of Agriculture, Regions and Tourism Stubenring 1, 1010 Vienna, 2021. ([https://www.world-mining-data.info/?World\\_Mining\\_Data\\_PDF-Files](https://www.world-mining-data.info/?World_Mining_Data_PDF-Files)).
- [9] H. Liu, K. Liu, Z. Lan, D. Zhang, Mechanical and electrical characteristics of graphite tailing concrete, Adv. Mater. Sci. Eng. 2018 (2018), <https://doi.org/10.1155/2018/9297628>.
- [10] Y. Duan, L. Niu, Y. He, K. neng Lei, X. Xu, C. li Zheng, C. Xiao, Effectiveness and mechanism of cyanide tailings cementation by steel slag coupled with non-ureolytic microbially induced carbonate precipitation, Process Saf. Environ. Prot. 190 (2024) 162–172, <https://doi.org/10.1016/j.psep.2024.07.016>.
- [11] K.R.M. Vieira, G.L.A.F. Arce, C.M.R. Luna, V.O. Facio, J.A. Carvalho, T.G.S. Neto, I. Ávila, Understanding the acid dissolution of Serpentinites (Tailings and waste rock) for use in indirect mineral carbonation, S Afr. J. Chem. Eng. 40 (2022) 154–164, <https://doi.org/10.1016/j.sajce.2022.02.005>.
- [12] S. Surehali, T. Han, J. Huang, A. Kumar, N. Neithalath, On the use of machine learning and data-transformation methods to predict hydration kinetics and strength of alkali-activated mine tailings-based binders, Constr. Build. Mater. 419 (2024), <https://doi.org/10.1016/j.conbuildmat.2024.135523>.
- [13] J. Xu, P. Chen, Synergistic effect of iron tailings, steel slag and red mud cementitious materials on mechanical and microstructure properties, J. Build. Eng. 95 (2024), <https://doi.org/10.1016/j.jobe.2024.110131>.
- [14] S. Maruthupandian, A. Chaliasou, A. Kanellopoulos, Recycling mine tailings as precursors for cementitious binders – methods, challenges and future outlook, Constr. Build. Mater. 312 (2021) 125333, <https://doi.org/10.1016/j.conbuildmat.2021.125333>.
- [15] • Graphite mine production top countries 2020 | Statista, (n.d.). (<https://www.statista.com/statistics/267366/world-graphite-production/>) (accessed February 23, 2022).
- [16] Z.R. Wang, B. Li, H.B. Liu, Y.X. Zhang, X. Qin, Degradation characteristics of graphite tailings cement mortar subjected to freeze-thaw cycles, Constr. Build. Mater. 234 (2020) 117422, <https://doi.org/10.1016/j.conbuildmat.2019.117422>.
- [17] Introduction to Climate Action | UNFCCC, (n.d.). (<https://unfccc.int/climate-action/introduction-climate-action>) (accessed August 16, 2023).
- [18] S. Bobba, S. Carrara, J. Huisman, F. Mathieux, C. Pavel, Critical Raw Materials for Strategic Technologies and Sectors in the EU - a Foresight Study, 2020. <https://doi.org/10.2873/58081>.
- [19] Critical raw materials, (n.d.). ([https://single-market-economy.ec.europa.eu/sectors/raw-materials/areas-specific-interest/critical-raw-materials\\_en](https://single-market-economy.ec.europa.eu/sectors/raw-materials/areas-specific-interest/critical-raw-materials_en)) (accessed August 14, 2023).
- [20] Z.R. Wang, B. Li, H.B. Liu, Y.X. Zhang, X. Qin, Degradation characteristics of graphite tailings cement mortar subjected to freeze-thaw cycles, Constr. Build. Mater. 234 (2020) 117422, <https://doi.org/10.1016/j.conbuildmat.2019.117422>.
- [21] H. Liu, Y. Zhang, B. Li, Z. Wang, Combined effects of graphite tailings and curing conditions on the early-age performances of cement mortar, Adv. Civ. Eng. 2020 (2020), <https://doi.org/10.1155/2020/5965328>.
- [22] Y. Peng, Y. Liu, B. Zhan, G. Xu, Preparation of autoclaved aerated concrete by using graphite tailings as an alternative silica source, Constr. Build. Mater. 267 (2021) 121792, <https://doi.org/10.1016/j.conbuildmat.2020.121792>.
- [23] J. Zheng, Y. Zhu, Z. Zhao, Utilization of limestone powder and water-reducing admixture in cemented paste backfill of coarse copper mine tailings, Constr. Build. Mater. 124 (2016) 31–36, <https://doi.org/10.1016/j.conbuildmat.2016.07.055>.
- [24] C.R. Wu, Z.Q. Hong, Y.H. Yin, S.C. Kou, Mechanical activated waste magnetite tailing as pozzolanic material substitute for cement in the preparation of cement products, Constr. Build. Mater. 252 (2020) 119129, <https://doi.org/10.1016/j.conbuildmat.2020.119129>.
- [25] L. Caneda-Martínez, C. Medina, M.I. Sánchez de Rojas, M. Frías, Water transport in binary eco-cements containing coal mining waste, Cem. Concr. Compos 104 (2019) 103373, <https://doi.org/10.1016/j.cemconcomp.2019.103373>.
- [26] C. Ince, Reusing gold-mine tailings in cement mortars: mechanical properties and socio-economic developments for the Lefke-Xeros area of Cyprus, J. Clean. Prod. 238 (2019) 117871, <https://doi.org/10.1016/j.jclepro.2019.117871>.
- [27] Y. Cheng, F. Huang, S. Qi, W. Li, R. Liu, G. Li, Durability of concrete incorporated with siliceous iron tailings, Constr. Build. Mater. 242 (2020) 118147, <https://doi.org/10.1016/j.conbuildmat.2020.118147>.
- [28] M.A. Longhi, E.D. Rodríguez, S.A. Bernal, J.L. Provis, A.P. Kirchheim, Valorisation of a kaolin mining waste for the production of geopolymers, J. Clean. Prod. 115 (2016) 265–272, <https://doi.org/10.1016/j.jclepro.2015.12.011>.
- [29] N. Sedira, J. Castro-Gomes, M. Magrinho, Red clay brick and tungsten mining waste-based alkali-activated binder: Microstructural and mechanical properties, Constr. Build. Mater. 190 (2018) 1034–1048, <https://doi.org/10.1016/j.conbuildmat.2018.09.153>.
- [30] P.H.R. Borges, F.C.R. Ramos, T.R. Caetano, T.H. Panzerra, H. Santos, Reuse of iron ore tailings in the production of geopolymer mortars, Rev. Esc. De. Minas 72 (2019) 581–587, <https://doi.org/10.1590/0370-44672017720169>.
- [31] L. Caneda-Martínez, C. Medina, M.I. Sánchez de Rojas, M. Frías, Water transport in binary eco-cements containing coal mining waste, Cem. Concr. Compos 104 (2019) 103373, <https://doi.org/10.1016/j.cemconcomp.2019.103373>.
- [32] Y. Cheng, F. Huang, S. Qi, W. Li, R. Liu, G. Li, Durability of concrete incorporated with siliceous iron tailings, Constr. Build. Mater. 242 (2020) 118147, <https://doi.org/10.1016/j.conbuildmat.2020.118147>.
- [33] G. Yao, Q. Liu, J. Wang, P. Wu, X. Lyu, Effect of mechanical grinding on pozzolanic activity and hydration properties of siliceous gold ore tailings, J. Clean. Prod. 217 (2019) 12–21, <https://doi.org/10.1016/j.jclepro.2019.01.175>.
- [34] The Munsell Color System, (n.d.). (<http://www.applepainter.com/>) (accessed July 4, 2022).
- [35] H. Shin, S. Lee, H. Suk Jung, J.B. Kim, Effect of ball size and powder loading on the milling efficiency of a laboratory-scale wet ball mill, Ceram. Int 39 (2013) 8963–8968, <https://doi.org/10.1016/j.ceramint.2013.04.093>.
- [36] P. Perumal, K. Piekari, H. Sreenivasan, P. Kinnunen, M. Illikainen, One-part geopolymers from mining residues – effect of thermal treatment on three different tailings, Min. Eng. 144 (2019) 106026, <https://doi.org/10.1016/j.mineng.2019.106026>.

- [37] A. Hajimohammadi, J.S.J. van Deventer, Dissolution behaviour of source materials for synthesis of geopolymer binders: a kinetic approach, *Int J. Min. Process* 153 (2016) 80–86, <https://doi.org/10.1016/j.minpro.2016.05.014>.
- [38] A. Hajimohammadi, J.L. Provis, J.S.J. Van Deventer, The effect of silica availability on the mechanism of geopolymerisation, *Cem. Concr. Res* 41 (2011) 210–216, <https://doi.org/10.1016/j.cemconres.2011.02.001>.
- [39] S. Ramanathan, REACTIVITY OF SUPPLEMENTARY CEMENTITIOUS MATERIALS IN MODEL SYSTEMS AND CEMENTITIOUS PASTES, PhD Thesis Submitted to University of Miami (2021) 249.
- [40] F. Avet, R. Snellings, A. Alujas, M. Ben, K. Scrivener, Cement and concrete research development of a new rapid, relevant and reliable (R3) test method to evaluate the pozzolanic reactivity of calcined kaolinitic clays, *Cem. Concr. Res* 85 (2016) 1–11, <https://doi.org/10.1016/j.cemconres.2016.02.015>.
- [41] F. Avet, R. Snellings, A. Alujas Diaz, M. Ben Haha, K. Scrivener, Development of a new rapid, relevant and reliable (R3) test method to evaluate the pozzolanic reactivity of calcined kaolinitic clays, *Cem. Concr. Res* 85 (2016) 1–11, <https://doi.org/10.1016/j.cemconres.2016.02.015>.
- [42] A. C1897-20, Standard Test Methods for Measuring the Reactivity of Supplementary Cementitious Materials by Isothermal Calorimetry and Bound Water, ASTM International, West Conshohocken, PA 04 (2020) 1–5. <https://doi.org/10.1520/C1897-20.2>.
- [43] S. Wang, Preparation of foam concrete from graphite tailing, *Adv. Mat. Res* 356–360 (2012) 1994–1997, <https://doi.org/10.4028/www.scientific.net/AMR.356-360.1994>.
- [44] H. Liu, B. Li, J. Xue, J. Hu, J. Zhang, Mechanical and electroconductivity properties of graphite tailings concrete, *Adv. Mater. Sci. Eng.* 2020 (2020), <https://doi.org/10.1155/2020/9385097>.
- [45] H. Liu, K. Liu, Z. Lan, D. Zhang, Mechanical and electrical characteristics of graphite tailing concrete, *Adv. Mater. Sci. Eng.* 2018 (2018), <https://doi.org/10.1155/2018/9297628>.
- [46] A. Sicakova, M. Kovac, Technological characterisation of selected mineral additives, *IOP Conf. Ser.: Mater. Sci. Eng., Construmet* (2018) 1–6, <https://doi.org/10.1088/1757-899X/385/1/012048>.
- [47] M. Kovac, A. Sicakova, M. Spak, Testing the Supplementary Cementitious Material Based on GGBFS and Zeolite for Prediction of the Activity Index, (2018) 1287. <https://doi.org/10.3390/proceedings2201287>.
- [48] C. Shi, P.V. Krivenko, D. Roy, *Alkali-Activated Cements and Concretes*, 03, CRC Press, 2003.
- [49] Lea's Chemistry of Cement and Concrete, Elsevier, 2019. <https://doi.org/10.1016/C2013-0-19325-7>.
- [50] K. Scrivener, R. Snellings, B. Lothenbach, *A Practical Guide to Microstructural Analysis of Cementitious Materials*, First ed., Taylor and Francis Group, 2016 (CRC Press).
- [51] L. Yu, Z. Zhang, X. Huang, B. Jiao, D. Li, Enhancement experiment on cementitious activity of copper-mine tailings in a geopolymer system, *Fibers* 5 (2017) 1–15, <https://doi.org/10.3390/fib5040047>.
- [52] X. Ren, L. Zhang, D. Ramey, B. Waterman, S. Ormsby, Utilization of aluminum sludge (AS) to enhance mine tailings-based geopolymer, *J. Mater. Sci.* 50 (2015) 1370–1381, <https://doi.org/10.1007/s10853-014-8697-y>.
- [53] Y. Chen, Y. Zhang, T. Chen, Y. Zhao, S. Bao, Preparation of eco-friendly construction bricks from hematite tailings, *Constr. Build. Mater.* 25 (2011) 2107–2111, <https://doi.org/10.1016/j.conbuildmat.2010.11.025>.
- [54] S. Luo, M. Liu, L. Yang, J. Chang, W. Yang, X. Yan, H. Yu, Y. Shen, Utilization of waste from alumina industry to produce sustainable cement-based materials, *Constr. Build. Mater.* 229 (2019) 116795, <https://doi.org/10.1016/j.conbuildmat.2019.116795>.
- [55] K. Peng, H. Yang, J. Ouyang, Tungsten tailing powders activated for use as cementitious material, *Powder Technol.* 286 (2015) 678–683, <https://doi.org/10.1016/j.powtec.2015.09.012>.
- [56] K. Berent, S. Komarek, R. Lach, W. Pyda, The Effect of Calcination Temperature on the Structure and Performance of Nanocrystalline Mayenite Powders, (2019).
- [57] X. Jiao, Y. Zhang, T. Chen, Thermal stability of a silica-rich vanadium tailing based geopolymer, *Constr. Build. Mater.* 38 (2013) 43–47, <https://doi.org/10.1016/j.conbuildmat.2012.06.076>.
- [58] K. Komnitsas, D. Zaharaki, Geopolymerisation: a review and prospects for the minerals industry, *Min. Eng.* 20 (2007) 1261–1277, <https://doi.org/10.1016/j.mineng.2007.07.011>.
- [59] Y.M. Liew, H. Kamarudin, A.M. Mustafa Al Bakri, M. Bnhussain, M. Luqman, I. Khairul Nizar, C.M. Ruzaidi, C.Y. Heah, Optimization of solids-to-liquid and alkali activator ratios of calcined kaolin geopolymeric powder, *Constr. Build. Mater.* 37 (2012) 440–451, <https://doi.org/10.1016/j.conbuildmat.2012.07.075>.
- [60] I. Silva, J.P. Castro-Gomes, A. Albuquerque, Effect of immersion in water partially alkali-activated materials obtained of tungsten mine waste mud, *Constr. Build. Mater.* 35 (2012) 117–124, <https://doi.org/10.1016/j.conbuildmat.2012.02.069>.
- [61] R. Ellerbrock, M. Stein, J. Schaller, Comparing amorphous silica, short-range-ordered silicates and silicic acid species by FTIR, *Sci. Rep.* 12 (2022), <https://doi.org/10.1038/s41598-022-15882-4>.
- [62] I.O. Faniyi, O. Fasakin, B. Olofinjana, A.S. Adekunle, T.V. Oluwasusi, M.A. Eleruja, E.O.B. Ajayi, The comparative analyses of reduced graphene oxide (RGO) prepared via green, mild and chemical approaches, *SN Appl. Sci.* 1 (2019) 1–7, <https://doi.org/10.1007/s42452-019-1188-7>.
- [63] S. Hollanders, Mineral. Study pozzolanic Prop. calcined clays (2017) 236. ([https://limo.libis.be/primo-explore/fulldisplay?docid=LIRIAS1727587&context=L&vid=Lirias&search\\_scope=Lirias&tab=default\\_tab&lang=en\\_US&fromSitemap=1](https://limo.libis.be/primo-explore/fulldisplay?docid=LIRIAS1727587&context=L&vid=Lirias&search_scope=Lirias&tab=default_tab&lang=en_US&fromSitemap=1)).
- [64] N. Sedira, J. Castro-Gomes, Effect of activators on hybrid alkaline binder based on tungsten mining waste and ground granulated blast furnace slag, *Constr. Build. Mater.* 232 (2020) 117176, <https://doi.org/10.1016/j.conbuildmat.2019.117176>.
- [65] D. Zhou, Developing Supplementary Cementitious Materials From Waste London Clay, Imperial College London (2016) 236. (<https://spiral.imperial.ac.uk/handle/10044/1/44528>).
- [66] H. Niu, P. Kinnunen, H. Sreenivasan, E. Adesanya, M. Illikainen, Structural collapse in phlogopite mica-rich mine tailings induced by mechanochemical treatment and implications to alkali activation potential, *Min. Eng.* 151 (2020) 106331, <https://doi.org/10.1016/j.mineng.2020.106331>.
- [67] S. Ramanathan, L.R. Pestana, P. Suraneni, Reaction kinetics of supplementary cementitious materials in reactivity tests, *Cement* 8 (2022) 100022, <https://doi.org/10.1016/j.cement.2022.100022>.
- [68] P.P. Sivakumar, S. Matthys, N. De Belie, E. Gruyaert, Reactivity assessment of modified ferro silicate slag by R3 method, *Appl. Sci.* 11 (2021) 1–14, <https://doi.org/10.3390/app11010366>.